

INVESTIGATION OF HYBRID ORGANIC-INORGANIC DIHYDROGEN PHOSPHATE BY HIRSHFELD SURFACE ANALYSIS AND QUANTUM CHEMICAL ANALYSIS

Abdellatif Rafik¹, , Hafid Zouihri², Taoufiq Guedira¹

<https://doi.org/10.23939/chcht17.02.244>

Abstract. This present work undertakes the study of organic-inorganic hybrid material, which has been obtained successfully by an acid-base reaction at room temperature and structurally studied by the single crystal X-ray diffraction method. N-(Dicyclopropylmethylamino)-4,5-dihydro-1,3-oxazolium dihydrogenphosphate [10-CN@DP] crystallizes in the triclinic system with the space group P-1. The X-ray structural analysis supported by a Hirshfeld surface analysis of the crystal structure indicates that the most significant contributions to the crystal packing are from H...H (63.3 %), H...O/O...H (32.2 %) and H...C/C...H (2.5 %) contacts. Density functional theory geometry-optimized calculations were compared to the experimentally determined structure. Using the same level of theory to imagine the chemical reactivity and charge distribution on the molecule, used to determine the HOMO-LUMO energy gap and density of state (DOS) range, the molecular electrostatic potential (MEP) image was drawn.

Keywords: HOMO–LUMO, density of state, Hirshfeld surface analysis, electrostatic potential surface.

1. Introduction

In recent years, nonlinear optical (NLO) materials have been the subject of intense research by chemists, material scientists and optical physicists owing to NLO potential application in various engineering technological fields.¹⁻⁶ This paper is a part of the systematic investigation of organic-inorganic hybrid materials including

amines and various mineral acids. The formation of the $(\text{H}_2\text{PO}_4^-)_n$ polyanion in the hybrid compound is interesting for chemists investigating new materials with optical properties, and biological or pharmacological drugs.⁴⁻¹⁰ Hybrid material described here contains different organic electron donors and the H_2PO_4^- anions structural study is fascinating by a great diversity of interactions; it shows clearly the strong and various hydrogen bonds between anions and cations. An inorganic-organic hybrid material is a fertile research topic that combines the advantages of organic components with those of an inorganic network (chemical, thermal and mechanical stability) (straightforward synthetic approach, easily tailored molecular structure and functional properties). With this view, an amino acid is chosen as a convenient basis to react with phosphoric acid, in which the basic nitrogen can retain a proton abstracted from the phosphate and the positive charge produced can contribute to the coulombic force of the crystal. In addition, the amine group can freely participate in the interaction of hydrogen bonding with phosphate. In the entire visible region, the resulting crystal is expected to have high lattice capacity, thermal stability, and negligible light absorption.

In the present investigation, the crystal structure of 10-CN@DP was examined by the computational chemical methods used to determine the energies of the atoms or molecules and other associated physical properties. In this study, Hartee-Fock (HF) and Density Functional Theory (DFT) with 6-31G basis set were used in the calculations of geometric structure and vibration frequencies of the studied compound. Additionally, the molecular geometrical parameters, the energies of the highest occupied molecular orbital (HOMO), and the lowest unoccupied molecular orbital (LUMO) were studied. Meanwhile, molecular electrostatic potential (MEP), and the main intermolecular interactions obtained from Hirshfeld study, Mulliken population study, which cannot be obtained experimentally, were performed.

¹ Laboratory of Organic Chemistry, Catalysis and Environment Laboratory, Faculty of Sciences, Ibn Tofail University, B.P. 133, 14000, Kenitra, Morocco

² Laboratory of Chemistry of Materials and Biotechnology of Natural Products, University Moulay Ismail, Faculty of Sciences, Meknes, Morocco

 abdellatif.rafik@uit.ac.ma

© Rafik A., Zouihri H., Guedira T., 2023

2. Experimental

2.1. Quantum Chemical Calculations

Using the Crystal Explorer 3.0 package,¹¹ the Hirshfeld surface and fingerprint plots of the synthesized compound were obtained. With color scale range of -0,908 a.u. (blue) and 1,497 a.u. (red), the d_{norm} graphs were mapped. The closest interactions between the atoms called in the compound units are shown by the red spots on the Hirshfeld surface. Using the extended 0.99–2.5 Å, the 2D fingerprint plots were shown. Molecular geometry optimization and all quantum-chemical calculations were performed using the B3LYP/6-31 G hybrid method with the software package Gaussian 09¹² and the molecular visualization application Gauss-View.¹³ As a result of hyper-conjugative interactions and electron delocalization, crystal stability was studied using the DFT method, geometry optimizations, electrostatic potential surface (ESP), HOMO-LUMO energies, and atomic charge distribution.

3. Results and Discussion

3.1. Single Crystal X-Ray Diffraction Study

The single crystal XRD investigation revealed that 10-CN@DP corresponds to the monoclinic system having space group P-1, the lattice parameter values a , b , c , and the volume of the unit cell, which are enumerated in Table 1, represent no modulation in crystal structure and are in accordance with literature data.¹⁴ The X-ray geometry of the monohydrogenphosphate anion HPO_4^{2-} , differs slightly from the optimized results (Fig. 1). In particular, the single P—OH bond is significantly longer (0.145 Å) in the optimized HPO_4^{2-} anion than in the crystal. The differences in the P—O distances for equivalent bonds in the H_2PO_4^- and HPO_4^{2-} anions correlate with the number and strength of the hydrogen bonds, in which the O atoms are involved.

The monohydrogenphosphate anion, HPO_4^{2-} , is involved in nine hydrogen bonds: as acceptor H in eight of them and as donor H – in one. The HPO_4^{2-} anion forms hydrogen bonds as acceptor H with four $\text{C}_{10}\text{H}_{17}\text{N}_2\text{O}^+$ residues *via* their amine H atoms, forming two hydrogen bonds with one $\text{C}_{10}\text{H}_{17}\text{N}_2\text{O}^+$ residue (*via* an amine H atom and the H atom at the protonated ring N atom), and with two H_2PO_4^- anions, and acts as a donor H to atom O₂ of one H_2PO_4^- anion (Fig. 2).

Table 1. Crystallographic data of 10-CN@DP

Crystal data	10-CN@DP
<i>Chemical formula</i>	$\text{C}_{10}\text{H}_{17}\text{N}_2\text{O}^+, \text{H}_2\text{PO}_4^-$
<i>Cell setting</i>	Triclinic
<i>Space group</i>	P-1
<i>a</i> (Å)	8.3212(8)
<i>b</i> (Å)	8.9609(9)
<i>c</i> (Å)	9.8813(10)
α (°)	97.070(2)
β (°)	101.475(2)
γ (°)	108.355(2)
<i>Z</i>	2
Volume (Å ³)	671.538

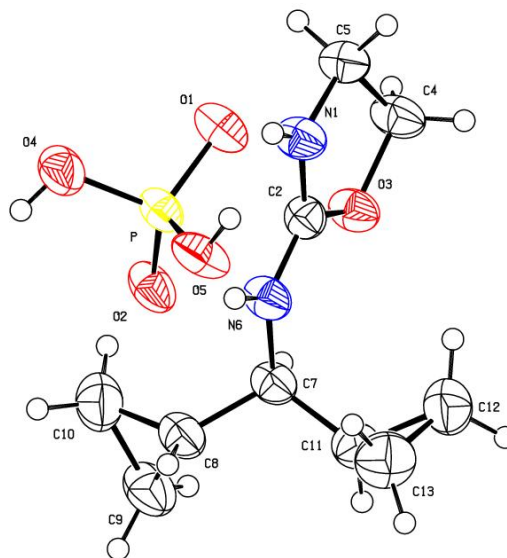


Fig. 1. A view of the molecular structure of 10-CN@DP, showing displacement ellipsoids drawn at the 30 % probability level

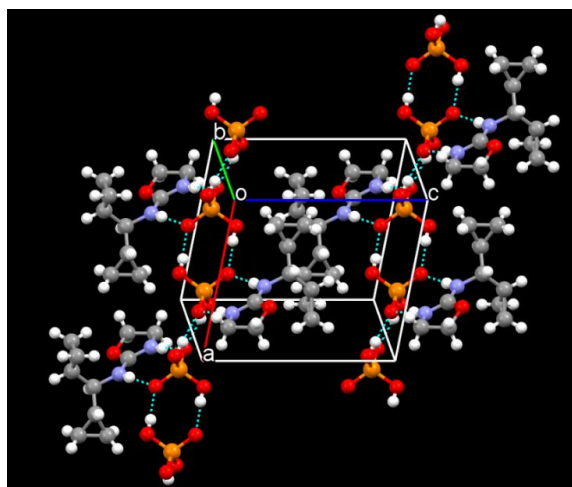


Fig. 2. Partial crystal packing of 10-CN@DP showing a chain of N-H...O hydrogen bonded molecules (intra- and intermolecular hydrogen bonds are indicated by dashed lines)

3.2. Hirshfeld Surface and 2D Fingerprint Print Analyses

Hirshfeld surfaces and their associated two-dimensional fingerprint plots¹⁵ were used to quantify the various intermolecular interactions in the title compound. The Hirshfeld surface map of a molecule is mapped using the descriptor d_{norm} which encompasses two factors: one is d_e , representing the distance of any surface point nearest to the internal atoms, and the other one is d_i , representing the distance of the surface point nearest to the exterior atoms and also with the van der Waals radii of the atoms.¹⁶

Using Crystal Explorer 3.0, Hirshfeld surfaces mapped over d_{norm} , shape index, and curvedness for the title compound were obtained to provide a better understanding of the molecular structure (Fig. 3). The internal and external (d_i and d_e) contact distances from the Hirshfeld surface to the nearest atom inside and outside allow the study of the intermolecular interactions through the mapping of d_{norm} .

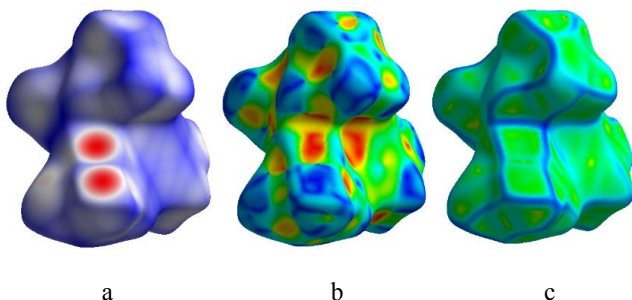


Fig. 3. Hirshfeld surface mapped over (a) d_{norm} , (b) shape-index and (c) curvedness

The red spots on the Hirshfeld surface of the compound 10-CN@DP indicate the presence of intermolecular interactions (intercontacts) in the crystalline setting of the title compound (Fig. 4, left). The Hirshfeld surface over d_{norm} suggests that pi-stacking interactions are the intermolecular interactions between the compound names, and the units are stacked, one above the other, in head-to-tail configuration. There is an intermolecular distance of 3.31 Å between the stacked units and a distance of 1.065 Å between the phosphate groups (Fig. 4).

The two-dimensional fingerprint plots for most of the intercontacts of the title compound are shown in Fig. 5 and summarized in Table 2. The highest interatomic contact contributions were found between hydrogen atoms H...H, at 63.3 %, followed by O...H/H...O and C...H/H...C, with contributions of 32.2 and 2.5 %, respectively.

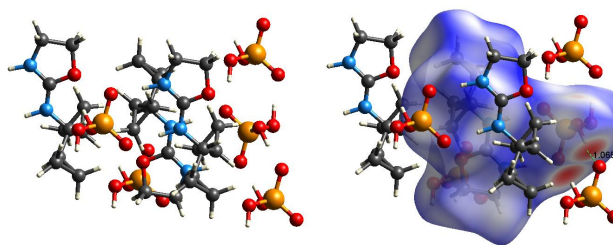


Fig. 4. d_{norm} mapped on the Hirshfeld surface plot of 10-CN@DP

Fig. 6 illustrates the view of the electrostatic potentials on Hirshfeld surface. Here, the red regions (visual intermolecular interaction acceptors) around the participating atoms correspond to the negative surface electrostatic potential. Likewise, the blue regions (visual of intermolecular interaction donors) lead to a positive surface electrostatic potential. In the 0.1067 to 0.1435 a.u. range, the electrostatic potential map was obtained. For the title compound, the STO-3 G basis set (Hartree-Fock method) was used. The red region above the O₁ atom included in the N-H...O hydrogen bond is related to the electrostatic potential of negative (hydrogen bond acceptors).

Where the void surface meets the boundary of the unit cell, capping faces are generated to create an enclosed volume. The term “voids” has been used in many different contexts when discussing the structure of crystalline materials, as well as visualizing voids for this compound. Crystal Explorer also reports the void surface. To answer this, we have computed void for this organic–inorganic hybrid compound with isovalue: 0.002 a.u. (corresponding approximately to a smoothed van der Waals surface); the resulting void surface, with a volume of 248.73 Å³ per unit cell (this value is remarkably close to the % void volume of 11.99 % described by the 0.002 a.u. void surface) and its surface area of 739.13 Å². The presence of voids and their distribution throughout the unit cell can largely determine the response of molecular crystals to external pressure.¹⁷ We have focused on this new approach to mapping voids in crystals (Fig. 7). On the Hirshfeld surface, some functions can be mapped, as these quantitatively authenticated observations display the effectiveness to gain insights into the intermolecular interactions in the context of crystal engineering.

Table 2. Summary of the closest contacts and their percentage contributions to the Hirshfeld surface

Type of contact	Contribution (%)
H...H	63.3
O...H/H...O	32.2
H...C/C...H	2.5
N...H/H...N	1.3
O...O	0.6

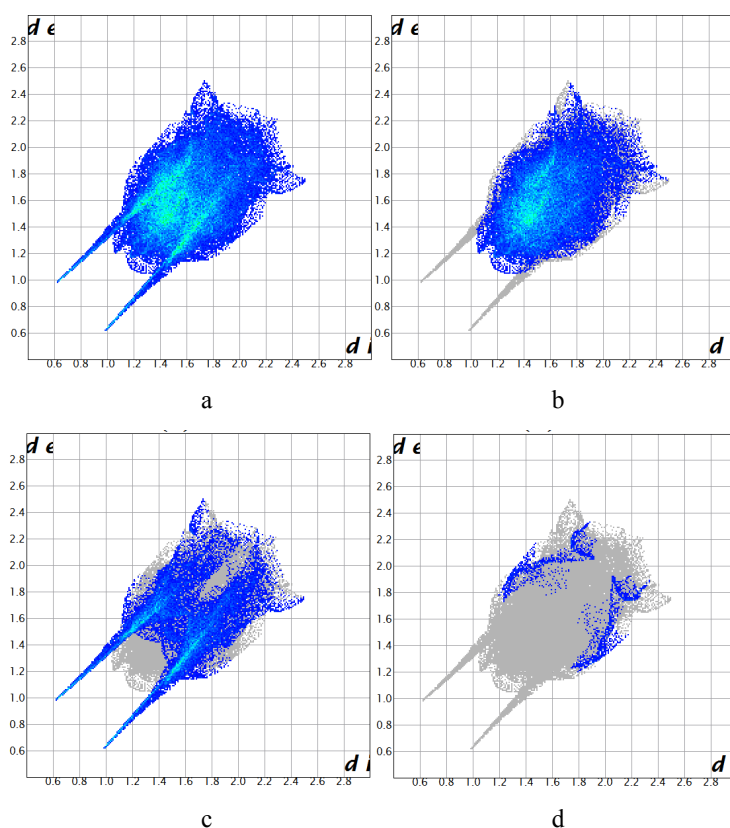


Fig. 5. The two-dimensional fingerprint plots for the title compound showing (a) all interactions, and delineated into (b) H...H, (c) H...O/O...H and (d) H...C/C...H. The d_i and d_e values are the closest internal and external distances (in Å) from given points on the Hirshfeld surface

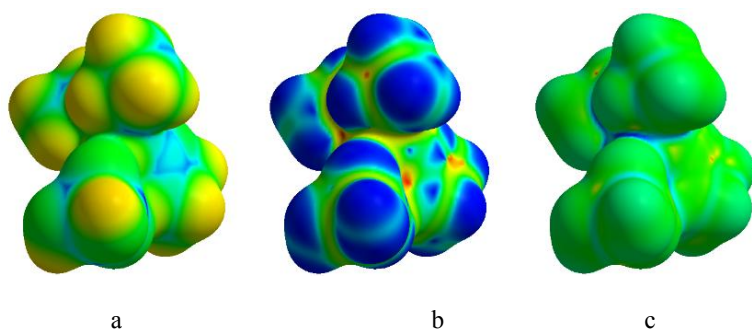


Fig. 6. Electrostatic potentials (EP) mapped on Hirshfeld surface with (a) d_i , (b) shape index and (c) curvedness of compound 10-CN@DP

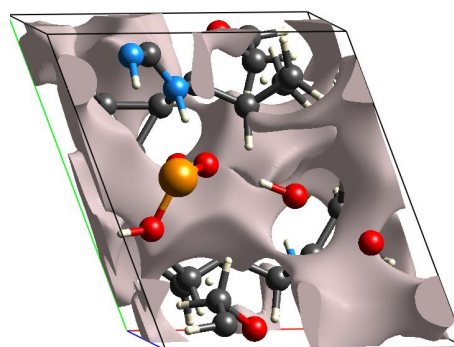


Fig. 7. Empty regions of the crystal structure of the molecule

3.3. Theoretical Studies

3.3.1. Optimized Molecular Structure by DFT Calculations

The optimized structure of the studied compound, namely 10-CN@DP, was obtained with the help of DFT calculation and HF methods.^{18,19} The mentioned opti-

mized structure obtained using B3LYP hybrid functional is given in Fig. 8. In Table 3, geometrical parameters such as bond length related to the studied compound are presented in detail. It is apparent from Table 3 that the experimental and theoretical results are in good agreement. It can be said that the minor deviations between theoretical and experimental results are due to the differences in the molecular environment. It should be noted that XRD

results were obtained in the crystalline phase. On the other hand, theoretical calculations were made in the gas phase using Gaussian Program. Note that experimental and theoretically obtained geometric parameter values are very close to each other (for example C₁₅-N₉ bond length values are 1.4576 and 1.4612 Å, respectively).

Table 3. Bond distances (Å) as well as the configurations in some selected dichromate compounds for comparison

Geometric Parameters	Experimental [X-ray]	Theoretical [DFT]	Theoretical [HF]
Bonds Å			
R(1,2)	1.5044	1.6138	1.5867
R(1,3)	1.5053	1.6163	1.5876
R(1,4)	1.5636	1.7320	1.6810
R(1,5)	1.5599	1.7312	1.6809
R(2,36)	1.8693	1.5528	1.6335
R(3,37)	1.9149	1.5916	1.6656
R(4,6)	0.8114	0.9805	0.9519
R(5,7)	0.8138	0.9805	0.9519
R(8,11)	1.3230	1.3781	1.3443
R(8,12)	1.4680	1.4950	1.4678
R(9,11)	1.3079	1.3360	1.3192
R(9,15)	1.4576	1.4723	1.4612
R(9,36)	0.8571	1.0684	1.0322
R(10,11)	1.3055	1.3146	1.2966
R(10,18)	1.4755	1.4866	1.4766
R(10,37)	0.8489	1.0628	1.0294
R(12,13)	0.9702	1.0884	1.0749
R(12,14)	0.9697	1.0918	1.0758
R(12,15)	1.5081	1.5464	1.5431
R(15,16)	0.9701	1.0923	1.0789
R(15,17)	0.9699	1.0958	1.0798
R(18,19)	0.9795	1.0958	1.0814
R(18,20)	1.5043	1.5223	1.5134
R(18,28)	1.5095	1.5276	1.5195
R(20,21)	0.9798	1.0868	1.0741
R(20,22)	1.4966	1.5190	1.5056
R(20,25)	1.4885	1.5165	1.5032
R(22,23)	0.9695	1.0865	1.0743
R(22,24)	0.9708	1.0847	1.0725
R(22,25)	1.4883	1.5204	1.5075
R(25,26)	0.9702	1.0863	1.0742
R(25,27)	0.9696	1.0847	1.0724
R(28,29)	0.9804	1.0877	1.0749
R(28,30)	1.4953	1.5171	1.5052
R(28,33)	1.4811	1.5196	1.5057
R(30,31)	0.9697	1.0853	1.0732
R(30,32)	0.9702	1.0855	1.0728
R(30,33)	1.4902	1.5211	1.5071
R(33,34)	0.9698	1.0853	1.0731
R(33,35)	0.9699	1.0859	1.0728

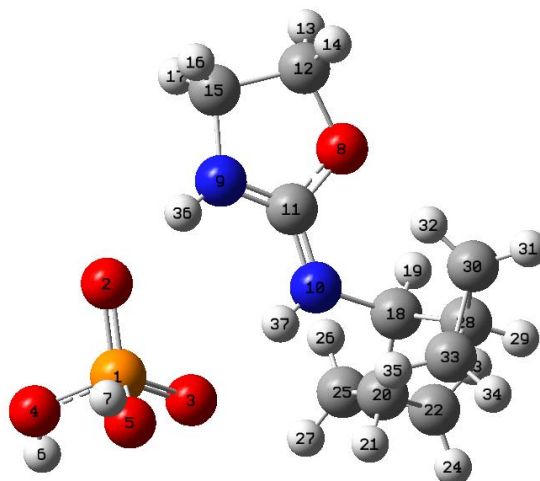


Fig. 8. Optimized molecular structure of 10-CN@DP compound

3.3.2. Mulliken Population Analysis

The corresponding Mulliken population, shown in Fig. 10, is a very accurate method of computational calculation for the microscopic system due to atomic charges that affect the dipole moment of 10-CN@DP molecules, which exhibit positive charges, while C₃₀, C₂₈, N₉, N₁₀, O₈, O₄, O₅, O₃ and O₂ atoms exhibit negative charges (Fig. 9). The charge transfers with basis set presumably occur due to polarization. The maximum negative charge values of O₃ atom by HF/B3LYP have a maximum positive charge value of P-1 atom around 1.9421 and 1.4127(e) in the molecule at HF and DFT, respectively. The Mulliken population analysis for 10-N@DP molecule was determined using B3LYP level with 6-31G basis set.²⁰ The charge distribution of the compound reveals that the substituted carbon atoms (C₁₂, C₁₁, C₁₅, C₁₈, C₂₀ and C₃₃) are positive while the remaining carbon atoms are negatively charged. This clearly represents that the delocalization of electrons from the nitrogen and carbon atoms of amine and methyl groups hallmarks the positive charge of the carbon atom. All hydrogen atoms are positively charged.

In addition, Mulliken atomic charges also show that the H atoms bonded to nitrogen and oxygen atoms (NH₃⁺ or H₂PO₄⁻ groups) have bigger positive atomic charges than the hydrogen attached to carbon atoms. This is due to the presence of N and O electronegative atoms. The highest positive charge (+1.199551(e)) associated with the phosphorus, is shown in (Fig. 10). It is the heaviest atom, which is surrounded by four oxygen atoms. The strongly negative charges are concentrated on nitrogen and oxygen atoms of amine group, which are involved as acceptors in hydrogen bonds. These results confirm the presence of a charge transfer through the N-H...O and

O-H...O hydrogen bonds, respectively. Furthermore, according to HF method the carbon O₂ and O₃ atoms (-0.968156 and -0.974587(e)) have higher electronegativity than other carbon atoms because they are surrounded by three electropositive hydrogen atoms.

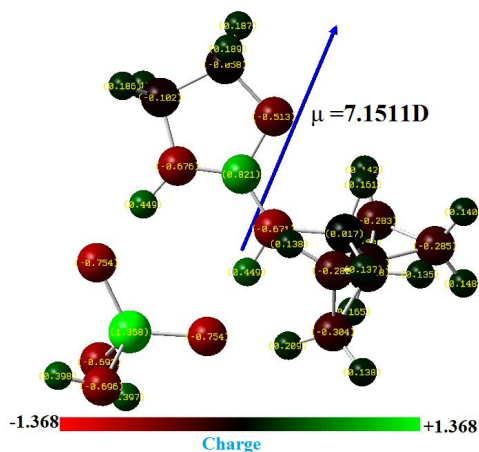


Fig. 9. Atomic charges distributions along with dipole moments orientations computation performed at the level of DFT theory (B3LYP/6-31)

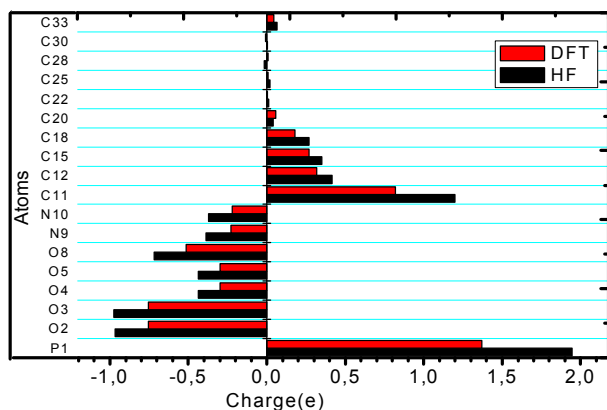


Fig. 10. Natural population charge of 10-CN@DP

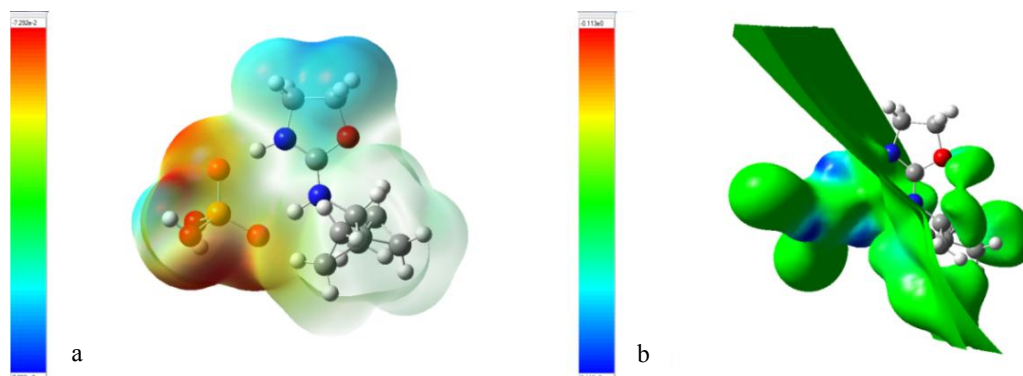


Fig. 11. (a) Molecular electrostatic potential and (b) electrostatic potential surface

3.3.3. Molecular Electrostatic Potential Surface Analysis

The MEP surface was drawn by the B3LYP/6-31G and HF methods.^{21,22} The surface immediately depicts the chemical reactivity scale, shape, charge, density, and location. It clarifies a visible technique to consider the relative polarity of the molecule and different values of the surface electrostatic potential expressed by dissimilar colors. In the row orange < yellow < blue < green,^{23,24} the electrostatic potential increases. Orange means the region with the most negative electrostatic potential, blue means the region with the most positive electrostatic potential, and green means zero potential. The light blue is a slightly electro-deficient region; the yellow region is slightly electron-made. The existence dominance of a light green area in the MESP surface corresponds to a possible halfway between two extremes of orange and blue color. The color code of these maps ranges from $-7.292e^{-2}$ and $+7.292e^{-2}$ eV, where blue indicates the strongest attraction and red indicates repulsion. The MEPs of title compounds presented in Fig. 11 clearly indicate that the phosphate oxygen atom 1, 2 and 3, as well as 4 oxygen atoms, contribute to the most electronegative region (red). Due to the excess of a negative charge, a relatively high nucleophilic activity of this part of the molecule can be expected. This is consistent with the well-known fact that lone electron pairs belonging to the electronegative atoms in the molecule are commonly aligned with the negative regions of MEP. On the other hand, both hydrogen atoms bonded to an oxygen atom in $H_2PO_4^-$ and hydrogen atoms bonded to an oxygen atom in $C_{10}H_{17}N_2O^+$ were located at positive MEP values. The distribution of the natural charge (Fig. 11) complies with MEP results. The negative charge was primarily distributed over the oxygen atoms attached to the $C_{10}H_{17}N_2O^+$ part as expected, while the remainder of the negative natural charge is mostly delocalized over the C₁₁, N₉.

3.3.4. Global Reactivity and HOMO-LUMO Orbitals

Frontier orbital energies provide essential clues about the reactivity of organic and inorganic compounds.²⁵ HOMO and LUMO orbitals obtained for studied compounds using B3LYP functional are shown in Fig. 12. The highest occupied molecular orbital energy determines the electron-donating ability, whereas the lowest unoccupied molecular orbital energy provides information about the ability of a molecule to accept an electron.²⁶ Table 4 represents HOMO and LUMO energy values; as well as energy gap.

10-CN@DP has a more tendency to accept electrons than C₁₀H₁₆N₂O, whereas in contrast, H₃PO₄ has significantly higher electron-donating ability. Furthermore, 10-CN@DP has the highest value of E_{LUMO}, indicating its ability to accept electrons be higher than that of other amines (Table 4).

Frontier orbital energy gap, softness and chemical hardness are widely used parameters by physicists and chemists.²⁷ Frontier orbital energy gap ($\Delta E = E_{\text{HOMO}} - E_{\text{LUMO}}$) is one of the key factors determining the reactivity and stability of molecules. According to the maximum hardness principle, the chemical hardness defined as the resistance against change in the number of electrons of a chemical entity is a measure of stability. Hard molecules with high-energy gap values have low electron donation ability.²⁸ On the other hand, soft molecules give electrons easily to metal surfaces. Soft molecules with a small energy gap are very reactive. Chemical hardness and softness values of 10-CN@DP are 1.7758 and 0.5631 a.u., respectively. If compare the chemical hardness values of 10-CN@DP, it is seen that the molecule with a lower chemical hardness value has a higher reactivity. Koopmans theorem presents an alternative way to predict molecule electron affinity.²⁸ According to this theorem, the negative values of LUMO and HOMO orbital energies are approximately equal to the electron affinity and the ionization energy, respectively.

In the light of Koopmans theorem, for ionization energy, electron affinity, chemical hardness, electronegativity, chemical potential and softness, the following equations can be given.²⁸

$$EA = -E_{\text{LUMO}} \text{ and } IP = -E_{\text{HOMO}} \quad (1)$$

$$\chi = -\mu = (IP + EA) / 2 \quad (2)$$

$$n = (IP - EA) / 2 \quad (3)$$

$$\sigma = 1/n \quad (4)$$

The chemical potential was found to be 3.3891 eV for the studied compound. According to electrophilicity, Eqs. (5)–(6) rely on its chemical potential (or electronegativity) and chemical hardness.²⁹

$$\omega = \mu^2 / 2n = \chi^2 / 2n \quad (5)$$

$$\varepsilon = 1/\omega \quad (6)$$

Calculated electrophilicity and nucleophilicity for 10-CN@DP compound are 3.2340 eV⁻¹ and 0.3092 eV⁻¹, respectively. It should be noted that electrophilicity provides data on the ability of an electron to accept a molecule, whereas nucleophilicity is a Lewis basicity test.²⁷ DOS represents the number of states in unit energy interval and their contributions to the chemical bonding through the COOP diagrams (Fig. 13). The bonding, anti-bonding and nonbonding essence of the interaction of the two orbitals, atoms or groups, is expressed by the OPDOS. A positive value indicates a bonding relationship (due to the positive overlap population), a negative value indicates that there is an anti-bonding relationship (due to the negative overlap population), and a non-bonding interaction is indicated by a zero value. OPDOS diagrams display and compare the ligand donor-acceptor properties and check the non-bonding bonding. The PDOS is represented by the composition of the fragment orbitals belonging to the MO. The total density states of the molecules are shown by carbon-nitrogen in the state density (DOS) of the 10-CN@DP compound. The positive energy of the carbon-nitrogen DOS is greater than that of the negative energy values.^{30,31}

Table 4. Quantum chemical parameters of the compound 10-CN@DP obtained by DFT

Parameter	Value
	10-CN@DP
E _{HOMO} (eV)	-0.21780 a.u
E _{LUMO} (eV)	-0.01197 a.u
Ionization potential ($I = -E_{\text{HOMO}}$)	0.21780 a.u
Electron affinity ($A = -E_{\text{LUMO}}$)	0.01197 a.u
Gap Energy ($E_{\text{LUMO}} - E_{\text{HOMO}}$)	5.58410 eV
Electronegativity ($\chi = (I+A)/2$)	0.114885 a.u
Chemical hardness ($n = (I-A)/2$)	0.102915 a.u
Chemical softness ($S = 1/2n$)	0.0514575 a.u ⁻¹
Chemical potential ($\mu = -(I+A)/2$)	-0.114885 a.u
Electrophilicity index ($\omega = \mu^2/2n$)	0.00067 a.u

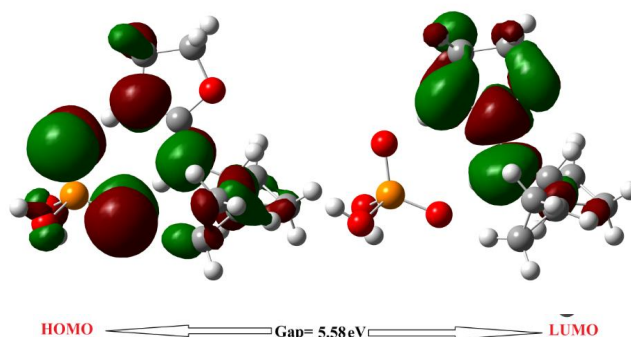


Fig. 12. The frontier molecular orbitals

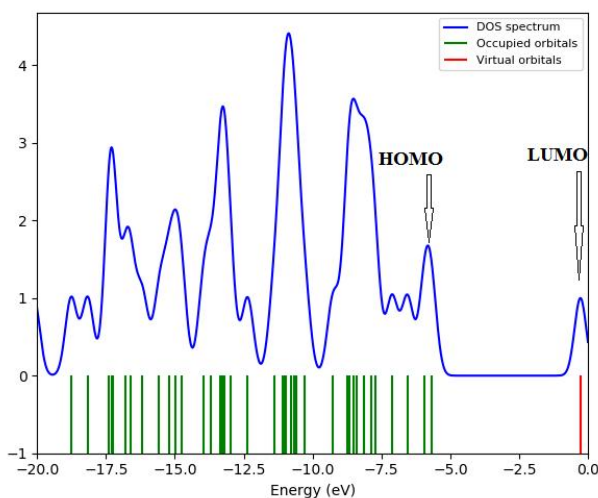


Fig. 13. Density of state (DOS) spectrum of 10-CN@DP compound

4. Conclusions

In summary, the structural property of hybrid organic-inorganic material containing 10-CN@DP was characterized. The XRD analysis confirmed the triclinic structural symmetry of the crystals and the unit cell parameters were determined. It is possible to characterize the structural arrangement of the title compound as an alternation of organic and inorganic layers along with the directions [101] and [110], made up of $[C_{10}H_{17}ON_2^+]$ and $[H_2PO_4^-]$ atom groups. The optimized geometric parameters (lengths of bonds, angles of bonds and angles of torsion) were theoretically calculated and compared with the experimental values. The HF and DFT methods were almost in agreement with the experimental findings, and no superiority was found between the methods. In addition, using the Mulliken population method with HF/6-31 G (d, p) and DFT / B3LYP/6-31 G basis sets, the net charge distribution of the title compound was determined. It was discovered from the Molecular Electrostatic Potential (MEP) map that the negative potential positions are on electronegative atoms, as well as the positive potential positions around the hydrogen atoms. These sites give information about the possible areas for inter and intermolecular hydrogen bonding. The findings of the MEP and Mulliken population methods were confirmed by the chemical active regions of each other. The values of electronegativity, chemical hardness and softness have been calculated. The stability and the cohesion of the structure were ensured by N-H...O hydrogen bonds. We also report a thorough study of the compound intermolecular interactions with the study of Hirshfeld surfaces and related fingerprint plots. The Hirshfeld surface study of the

crystal structure states that the most relevant contributions to crystal packing are from interactions between H...H / H...H (63.3 %), H...O / O...H (32.2 %) and H...C / C...H (2.5 %).

References

- [1] Guloy, A.M.; Tang, Z.J.; Miranda, P.B.; Srdanov, V.I. A New Luminescent Organic-Inorganic Hybrid Compound with Large Optical Nonlinearity. *Adv. Mater.* **2001**, *13*, 833-837. [https://doi.org/10.1002/1521-4095\(200106\)13:11%3C833::AID-ADMA833%3E3.0.CO;2-T](https://doi.org/10.1002/1521-4095(200106)13:11%3C833::AID-ADMA833%3E3.0.CO;2-T)
- [2] Chang, H.-Y.; Kim, S.-H.; Halasyamani, P.S.; Ok, K.M. Alignment of Lone Pairs in a New Polar Material: Synthesis, Characterization, and Functional Properties of $Li_2Ti(IO_3)_6$. *J. Am. Chem. Soc.* **2009**, *131*, 2426-2427. <https://doi.org/10.1021/ja808469a>
- [3] Chang, H.-Y.; Kim, S.-H.; Ok, K.M.; Halasyamani, P.S. New Polar Oxides: Synthesis, Characterization, Calculations, and Structure-Property Relationships in $RbSe_2V_3O_{12}$ and $TlSe_2V_3O_{12}$. *Chem. Mater.* **2009**, *21*, 1654-1662. <https://doi.org/10.1021/cm9002614>
- [4] Abu El-Fadl, A.; Gaffar, M.A.; Omar, M.H. Electrical Conductivity and Pyroelectricity of Lithium-Potassium Sulphate Single Crystal in the Temperature Range 300–950 K. *Physica B Condens. Matter* **1999**, *269*, 395-402. [https://doi.org/10.1016/S0921-4526\(99\)00116-7](https://doi.org/10.1016/S0921-4526(99)00116-7)
- [5] Horiuchi, S.; Tokunaga, Y.; Giovannetti, G.; Picozzi, S.; Itoh, H.; Shimano, R.; Kumai, R.; Tokura, Y. Above-room-temperature Ferroelectricity in a Single-Component Molecular Crystal. *Nature* **2010**, *463*, 789-792. <https://doi.org/10.1038/nature08731>
- [6] Mishurov, D.; Voronkin, A.; Roshal, A.; Bogatyrenko, S.; Vashchenko, O. Synthesis and Characterization of Dye-Doped Polymer Films for Non-linear Optical Applications. *Chem. Chem. Technol.* **2019**, *13*, 459-464. <https://doi.org/10.23939/chcht13.04.459>
- [7] Hearn, R.A.; Bugg, C.E. The crystal Structure of (-)-Ephedrine Dihydrogen Phosphate. *Acta. Crystallogr. B. Struct. Sci. Cryst. Eng. Mater.* **1972**, *B28*, 3662-3667. <https://doi.org/10.1107/S0567740872008532>
- [8] Adams, J.M. The Crystal Structure of Aminoguanidinium Dihydrogen Orthophosphate. *Acta. Crystallogr. B. Struct. Sci. Cryst. Eng. Mater.* **1977**, *B33*, 1513-1515. <https://doi.org/10.1107/S0567740877006402>
- [9] Rafik, A.; Zouhri, H.; Guedira, T. Analysis of H-Bonding Interactions with Hirshfeld Surfaces and Geometry-Optimized Structure of the DL-Valinium Dihydrogen Phosphate. *J. Chem. Technol. Metall.* **2021**, *56*, 275-282.
- [10] Blessing, R.H. Hydrogen Bonding and Thermal Vibrations in Crystalline Phosphate Salts of Histidine and Imidazole. *Acta. Crystallogr. B. Struct. Sci. Cryst. Eng. Mater.* **1986**, *B42*, 613-621. <https://doi.org/10.1107/S0108768186097641>
- [11] Wolff, S.K.; Grimwood, D.J.; McKinnon, J.J.; Turner, M.J.; Jayatilaka, D.; Spackman, M.A. *CrystalExplorer 3.0*; University of Western Australia, Perth, 2012.
- [12] Frisch, M.J.; Trucks, G.W.; Schlegel, H.B.; Scuseria, G.E.; Robb, M.A.; Cheeseman, J.R.; Scalmani, G.; Barone, V.; Petersson, G.A.; Nakatsuji, H. *et al. Gaussian*; Inc., Wallingford CT, 2016.
- [13] Dennington, R. II; Keith, T.; Millam, J. *GaussView*, Version 4.1. 2, Semichem Inc Shawnee Mission KS, 2007.

- [14] Guelmami, L.; Gharbi, A.; Jouini, A. 4-Dimethylaminopyridinium dihydrogenmonophosphate ($C_7H_{11}N_2$) H_2PO_4 : Synthesis, Structural, ^{31}P , ^{13}C NMR and Thermal Investigations. *J. Chem. Crystallogr.* **2012**, *42*, 549-554. <https://doi.org/10.1007/s10870-012-0277-x>
- [15] Marchewka, M. K.; Drozd, M.; Janczak, Ja. Crystal and Molecular Structure of *n*-(4-Nitrophenyl)- β -alanine—Its Vibrational Spectra and Theoretical Calculations. *Spectrochim. Acta A Mol. Biomol. Spectrosc.* **2011**, *79*, 758-766. <https://doi.org/10.1016/j.saa.2010.08.050>
- [16] Breda, S.; Reva, I.D.; Lapinski, L.; Nowak, M.J.; Fausto, R. Infrared Spectra of Pyrazine, Pyrimidine and Pyridazine in Solid Argon. *J. Mol. Struct.* **2006**, *786*, 193-206. <https://doi.org/10.1016/j.molstruc.2005.09.010>
- [17] Turner, M.J.; McKinnon, J.J.; Jayatilaka, D.; Spackman, M.A. Visualisation and Characterisation of Voids in Crystalline Materials. *CrystEngComm* **2011**, *13*, 1804-1813. <https://doi.org/10.1039/C0CE00683A>
- [18] Santhy, K.R.; Sweetlin, M.D.; Muthu, S.; Kuruvilla, T.K.; Abraham, C.S. Structure, Spectroscopic study and DFT Calculations of 2,6 bis (tri fluoro methyl) benzoic acid. *J. Mol. Struct.* **2019**, *1177*, 401-417. <https://doi.org/10.1016/j.molstruc.2018.09.058>
- [19] Chethan Prathap, K.N.; Lokanath, N.K. Three Novel Coumarin-Benzenesulfonylhydrazide Hybrids: Synthesis, Characterization, Crystal Structure, Hirshfeld Surface, DFT and NBO Studies. *J. Mol. Struct.* **2018**, *1171*, 564-577. <https://doi.org/10.1016/j.molstruc.2018.06.022>
- [20] Mulliken, R.S. Electronic Population Analysis on LCAO-MO Molecular Wave Functions. I. *J. Chem. Phys.* **1955**, *23*, 1833. <https://doi.org/10.1063/1.1740588>
- [21] Nataraj, A.; Balachandran, V.; Karthick, T. Molecular Orbital Studies (Hardness, Chemical Potential, Electrophilicity, and First Electron Excitation), Vibrational Investigation and Theoretical NBO Analysis of 2-Hydroxy-5-bromobenzaldehyde by Density Functional Method. *J. Mol. Struct.* **2013**, *1031*, 221-233. <https://doi.org/10.1016/j.molstruc.2012.09.047>
- [22] Onitsch, E.M. Uber die Mikroharthe der Metalle. *Mikroskopie* **1947**, *2*, 131.
- [23] Premkumar, S.; Jawahar, A.; Mathavan, T.; Kumara Dhas, M.; Sathe, V.G.; Benial, A.M.F. DFT Calculation and Vibrational Spectroscopic Studies of 2-(Tert-butoxycarbonyl (Boc) -amino)-5-bromopyridine. *Spectrochim. Acta A Mol. Biomol. Spectrosc.* **2014**, *129*, 74-83. <https://doi.org/10.1016/j.saa.2014.02.147>
- [24] Mathammal, R.; Sudha, N.; Prasad, L.G.; Ganga, N.; Krishnakumar, V. Spectroscopic (FTIR, FT-Raman, UV and NMR) investigation and NLO, HOMO-LUMO, NBO analysis of 2-Benzylpyridine based on quantum chemical calculations. *Spectrochim. Acta A Mol. Biomol. Spectrosc.* **2015**, *137*, 740-748. <https://doi.org/10.1016/j.saa.2014.08.099>
- [25] Uzun, S.; Esen, Z.; Koç, E.; Usta, N.C.; Ceylan, M. Experimental and Density Functional Theory (MEP, FMO, NLO, Fukui Functions) and Antibacterial Activity Studies on 2-Amino-4- (4-nitrophenyl) -5,6-dihydrobenzo [h] quinoline-3-carbonitrile. *J. Mol. Struct.* **2019**, *1178*, 450-457. <http://dx.doi.org/10.1016/j.molstruc.2018.10.001>
- [26] Attar, T.; Messaoudi, B.; Benhadria, N. DFT Theoretical Study of Some Thiosemicarbazide Derivatives with Copper. *Chem. Chem. Technol.* **2020**, *14*, 20-25. <https://doi.org/10.23939/chcht14.01.020>
- [27] Kaya, S.; Tüzün, B.; Kaya, C.; Obot, I.B. Determination of Corrosion Inhibition Effects of Amino Acids: Quantum Chemical and Molecular Dynamic Simulation Study. *J. Taiwan Inst. Chem. Eng.* **2016**, *58*, 528-535. <https://doi.org/10.1016/j.jtice.2015.06.009>
- [28] Lanez, E.; Bechki, L.; Lanez, T. Ferrocenylmethyl nucleobases: Synthesis, DFT Calculations, Electrochemical and Spectroscopic Characterization. *Chem. Chem. Technol.* **2020**, *14*, 146-153. <https://doi.org/10.23939/chcht14.02.146>
- [29] Parr, R.G.; Szentpaly, L.V.; Liu, S. Electrophilicity Index. *J. Am. Chem. Soc.* **1999**, *121*, 1922-1924. <https://doi.org/10.1021/ja983494x>
- [30] Pandey, M.; Muthu, S.; Nanje Gowda, N.M. Quantum Mechanical and Spectroscopic (FT-IR, FT-Raman, 1H , ^{13}C NMR, UV-Vis) Studies, NBO, NLO, HOMO, LUMO and Fukui Function Analysis of 5-Methoxy-1H-benzo[d]imidazole-2(3H)-thione by DFT Studies. *J. Mol. Struct.* **2017**, *1130*, 511-521. <https://doi.org/10.1016/j.molstruc.2016.10.064>
- [31] Gumus, S.; Sundius, T.; Yilmaz, V. Vibrational Analyses of 1,3-Dibenzoyl-4,5-dihydro-1H-imidazole-2-thione and 1,3-Dibenzoyl tetrahydropyrimidine-2(1H)-thione by Normal Coordinate Treatment. *Spectrochim. Acta A Mol. Biomol. Spectrosc.* **2012**, *98*, 384-395. <https://doi.org/10.1016/j.saa.2012.08.058>

Received: November 19, 2021 / Revised: February 19, 2022 / Accepted: May 06, 2022

ДОСЛІДЖЕННЯ ГІБРИДНОГО ОРГАНІЧНО-НЕОРГАНІЧНОГО ДИГІДРОФОСФАТУ ЗА ДОПОМОГОЮ ПОВЕРХНЕВОГО АНАЛІЗУ ЗА ХІРШФЕЛЬДОМ ТА КВАНТОВО-ХІМІЧНОГО АНАЛІЗУ

Анотація. У роботі вивчено органічно-неорганічний гібридний матеріал, який був успішно отриманий кислотно-основною реакцією за кімнатної температури та структурно вивчений методом рентгенівської дифракції монокристалів. *N*-(Дигідропропілметиламіно)-4,5-дигідро-1,3-оксазолію дигідрофосфат [10-CN@DP] кристалізується в триклінній системі з просторовою групою *P*-1. Рентгеноструктурний аналіз, підтверджений поверхневим аналізом кристалічної структури Хіршфельда, показує, що найбільший внесок у кристалічне упакування роблять $H...H$ (63,3%), $H...O/O...H$ (32,2%) і $H...C/C...H$ (2,5%) контакти. Розрахунки з використанням теорії функціонала густини, оптимізовані за геометрією, порівняно з експериментально визначеною структурою. Використовуючи той самий рівень теорії, створено зображення молекулярного електростатичного потенціалу (MEP), щоб відобразити хімічну реакційну здатність і розподіл заряду на молекулі, що використовується для визначення діапазону енергетичної щільності ВЗМО-НВМО та густини стану (DOS).

Ключові слова: ВЗМО-НВМО, густина стану, поверхневий аналіз Хіршфельда, поверхня електростатичного потенціалу.